# We are IntechOpen, the world's leading publisher of Open Access books Built by scientists, for scientists

**4,800**
Open access books available

**122,000**
International authors and editors

**135M**
Downloads

Our authors are among the

**154**
Countries delivered to

**TOP 1%**
most cited scientists

**12.2%**
Contributors from top 500 universities


WEB OF SCIENCE™

Selection of our books indexed in the Book Citation Index in Web of Science™ Core Collection (BKCI)

## Interested in publishing with us?
## Contact book.department@intechopen.com

Numbers displayed above are based on latest data collected.
For more information visit www.intechopen.com

Chapter 5

# Pulsed Laser-Deposited $TiO_2$-based Films: Synthesis, Electronic Structure and Photocatalytic Activity

Oksana Linnik, Nataliia Chorna, Nataliia Smirnova, Anna Eremenko, Oleksandr Korduban, Nicolaie Stefan, Carmen Ristoscu, Gabriel Socol, Marimona Miroiu and Ion N. Mihailescu

Additional information is available at the end of the chapter

http://dx.doi.org/10.5772/62637

**Abstract**

Active under visible light, photocatalysts based on doped titania were obtained via pulsed laser deposition (PLD) method. To find out the crystalline structure, optical properties, and electronic structure, the following techniques such as X-ray diffraction, electronic spectroscopy, electrical conductivity measurements, and X-ray photoelectron spectroscopy (XPS) are used. Photocatalytic activity is monitored by applying the photoreduction of dichromate ions under UV and visible light. The influence of zirconium ions and its content and synthesis conditions on the efficiency of nitrogen incorporation into titania structure that, in turn, determines the electronic structure and photocatalytic ability of the semiconductive materials are discussed. A substitutional nitrogen (Ti–N) rather than an interstitial one (Ti–O–N) is mainly responsible for the observed photoactivity. It is pointed that substitutional nitrogen is responsible for bandgap narrowing or formation of intragap localized states within semiconductor bandgap. The bandgap energy values are sharply decreased, while the relative intensity of substitutional nitrogen XPS peaks is increased. Pulsed laser synthesis of $TiO_2$ films in $N_2/CH_4$ atmosphere not only leads to nitrogen incorporation but also to the formation of defects including oxygen vacancies and $Ti^{3+}$ states which are all contributing to light absorption. An appropriate ratio of gas mixture, optimum zirconia content, suitable pressure, and temperature during synthesis was found for the synthesis of highly active semiconductive films. The highest photocatalytic conversion yields are obtained for nitrogen-doped 10% $ZrO_2/TiO_2$ synthesized in $N_2:CH_4 = 5:1$ at 100 Pa and at 450°C under both UV and visible light.

**Keywords:** photocatalysis, semiconductor, bandgap, nitrogen-doped titania, zirconia, pulsed laser deposition, substitutional and interstitial nitrogen, X-ray photoelectron spectroscopy

## 1. Introduction

Among the ways leading to the intensive climate change, the widespread contamination of air, soil, and water sources are to be considered. Titania is recognized as the most prospective photocatalyst used in air purification, surface self-cleaning, and wastewater treatment [1–7]. Since solar radiation includes light of wavelengths from 280 to 4000 nm, the use of titania that absorbs the edge (3–5%) of solar energy is not efficient. Many studies are performed to design and develop photocatalysts based on titania to allow for their use under visible-light irradiation [8, 9]. Nitrogen, the most promising among nonmetal dopants, facilitates visible light absorption by nanomaterials based on $TiO_2$ as a result of its incorporation into titania matrix due to its comparable atomic size with oxygen, small ionization energy, and high stability. Another approach to change the physical, optical, structural, and photocatalytic properties of titania includes employment of d-block metal ions (*e.g.*, zinc, zirconium, iron, chromium, nickel, vanadium, or copper).

An incorporation of zirconium ions in $TiO_2$ lattice was reported to enhance the specific surface area and the surface acidity and to modify the photo-electrochemical properties, leading to the improvement of the photocatalytic activity [10]. $Ti_{1-x}Zr_xO_2$ solid solution containing anatase led to the increase of bandgap energy with the anodic shift of the upper edge of the valence band position accelerating photocatalytic processes due to the improvement of charge separation. It was found an optimum content of $ZrO_2$ in $TiO_2$ that increased the quantity of the surface active sites such as OH-groups [11]. In the case of zinc-containing nanocomposites, their crystallinity slightly increased with Zn content and $ZnTiO_3$ perowskite phase is formed. The films with low Zn content (1–5 wt%) exhibited superhydrophilicity. Direct photo-electrochemical measurements showed the cathodic shift of the flat band potential position and the increase of the photocurrent quantum yield for $TiO_2$/ZnO in comparison with unmodified $TiO_2$ electrodes that coincided with the increase of their photocatalytic activity [11]. More effective degradation was observed for $Zn^{2+}$-doped samples with homogeneously distributed noble metal nanoparticles as a result of synergetic effect of new formed $Zn_2Ti_3O_8$ phase and the charge separation promoted by the noble metal nanoparticles. It was found that a higher dispersion of noble metal crystallization centers did occur near zinc ions in titania matrix [12, 13]. Nanostructured iron titanate and ruthenium-modified titania thin films are reported to catalyze the photocatalytic dinitrogen reduction that is the second, after photosynthesis, most important chemical process in nature. A detailed mechanism investigation clarified the role of metal ions in all complicated steps of this process [14, 15]. However, d-block metals may also act as recombination sites for the photo-induced charge carriers lowering the activity of the semiconductors. Despite the fact that a decrease in bandgap energy was achieved by metal doping, photocatalytic activity has not been remarkably enhanced [16].

http://dx.doi.org/10.5772/62637

Since Sato [17] reported the visible-light activity of N-doped titania in the oxidation of carbon monoxide and ethane, and later, Asahi [18] explored the visible-light activity of N-doped $TiO_2$, there have been many efforts dealing with nitrogen doping of $TiO_2$. Numerous physical techniques such as sputtering [19, 20] and ion implantation [21], atomic layer deposition [22], pulse laser deposition [23], gas phase reaction [24], and the sol–gel method [16] have been successfully applied to obtain nitrogen-modified $TiO_2$.

It is reported [18] that the doping of nonmetals could narrow the bandgap and might drive the response to visible light due to the similar energies of oxygen and nitrogen resulting in the hybridization of N 2p with O 2p states in anatase $TiO_2$. On the other hand, it is stated [25] that isolated impurity energy levels above the valence band are formed as a result of oxygen atoms substitution by nitrogen ones. Irradiation with UV light excites electrons in both the valence band (VB) and the impurity energy levels, but illumination with visible light only excites electrons in the impurity energy level. An alternative point of view, where the visible-light activation of anion-doped $TiO_2$ originates from the defects associated with oxygen vacancies, was also reported. As a result, the color centers appeared displaying these absorption bands, and not to a narrowing of the bandgap of $TiO_2$ [26]. Whereas surface oxygen vacancies were reduced considerably after reheating at 400°C, the activity of N-doped $TiO_2$ was enhanced fourfold suggesting no oxygen vacancies influence on visible-light activity [27]. In addition, nitrogen-modified titania powder obtained by mixing a commercially manufactured titania powder and the different nitrogen containing organic substances were applied for photomineralization of formic acid under visible light. It is concluded that neither nitridic nor $NO_x$ species nor defect states are responsible for the visible-light photocatalytic activity of modified titania prepared from urea, but higher melamine condensation products acting as visible-light sensitizers [28].

The main technique proving the nitrogen incorporation into a semiconductor structure as substitutional nitrogen atom ($N_s$), where nitrogen substitutes oxygen lattice ions or interstitial one ($N_i$), and N binds to O lattice ions, is X-ray photoelectron spectroscopy (XPS). There is no definite opinion about the XPS measurements of N1s binding energy (BE). The peak at 395.7 eV is assignable to $N^{3-}$ bonded to three Ti atoms because the measured binding energy is very close to that of titanium nitrides (ca. 396.0 eV) [29, 30]; the values of 396–397 eV are assigned to the N–Ti–N [31] or O–Ti–N bonds [32]. The formation of N–N or N–C, N–O groups or chemisorbed dinitrogen was suggested for higher energies of (400–402 eV) [33]. Note that N1s binding energies of 399.1 and 400.5 eV measured for modified by urea commercially available $TiO_2$ powder were assigned to carbon nitrides (399–400 eV, C=N–C), graphite-like phases (400.6 eV, N-C$sp^2$), and to polycyanogen (399.0, 400.5 eV $(–C=N–)_x$) [34]. XPS and electron paramagnetic resonance (EPR) measurements showed that the interstitial nitrogen atoms corresponded to BE of 400–401 eV are the photoactive species and can be prepared from discharge in molecular nitrogen in the presence of pure anatase [35]. However, the intensity of 400 eV peak belonged to the nitrogen atom from ammonium ions is reduced after rinsing as provided by XPS and solid-state nuclear magnetic resonance (NMR) [36].

The geometric structures of diamagnetic (**Scheme 1, i**) and paramagnetic (**Scheme 1, ii–vi**) nitrogen species incorporated into titania suggested from the literature were summarized in

Ref. [29]. Nitrogen species with a binding energy of ca. 396 eV represent TiN species (nitridation of titania) described as structure i, where $N^{3-}$ species are directly bonded to three $Ti^{3+}$ cations [29]. The N contained species corresponding to structure ii are related to a binding energy in the range of 397–399 eV [30, 37]. The formation of O–Ti–N–Ti during the synthesis could take place (structures iii and iv), when nitrogen substituted the lattice oxygen atom of O–Ti–O–Ti [38]. The structure v where the nitrogen atom connected with two oxygen of the $TiO_2$ lattice depicted as imino-type species and may be formed as a result of the incomplete reaction of ammonia with surface oxygen atoms [39]. It is believed [40] that the imino-type species undergoes to nitrate-type species (structure vi) where the last is the photoactive nitrogen species.

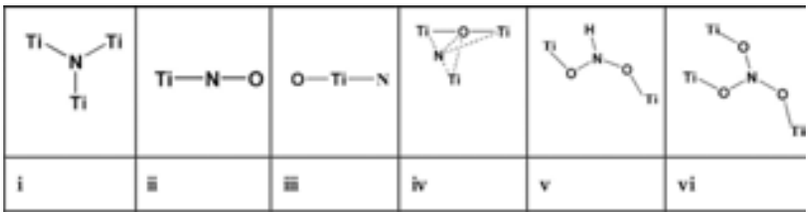


**Scheme 1.** Proposed structures of N species incorporated into titania as summarized in Ref. [29]. Reproduced with permission.

In light of numerous literature investigations, the applied synthesis conditions and the source of nitrogen are the turning points for the level of nitrogen doping and its states that change optical, electronic, and photocatalytic properties of a semiconductor.

The main principles of heterogeneous photocatalysis are presented as follows (**Figure 1**): (i) A semiconductor is characterized by an electronic band structure in which the highest occupied energy valence band (VB) and the lowest empty conduction band (CB) are separated by bandgap; (ii) only a photon of energy higher or equal to the bandgap energy (≥3.2 eV for anatase) promotes to a charge separation resulting in an electron ($e^-$) transferring from the VB to the CB with simultaneous generation of a hole ($h^+$) in the VB (pathway 1); (iii) an electron and a hole can be trapped in surface states and react with donor (D) and acceptor (A) species, respectively, adsorbed or close to the surface of the particle resulting in the simultaneous oxidation and reduction (pathways 1.1 and 1.2); or (iv) a photoformed electron–hole pair can be recombined (pathway 2) on the surface or in the bulk of the particle in a few nanoseconds. The energy level at the bottom of the CB is actually the reduction potential of photoelectrons and the energy level at the top of the VB determines the oxidizing ability of photoformed holes. The flat-band potential presents the energy of both charge carriers at the semiconductor–electrolyte interface and depends on the nature of the material and the system equilibrium.

From a thermodynamic point of view, the trapped electron reduces an electron acceptor only if its redox potential is more positive than the flat-band potential of the CB, while the trapped hole oxidizes the adsorbed species having the redox potential more negative than the flat-band potential of the VB. The visible-light photoactivity of metal-ions-doped $TiO_2$ can be explained by a new energy level produced in the bandgap where an electron can be excited from the

http://dx.doi.org/10.5772/62637

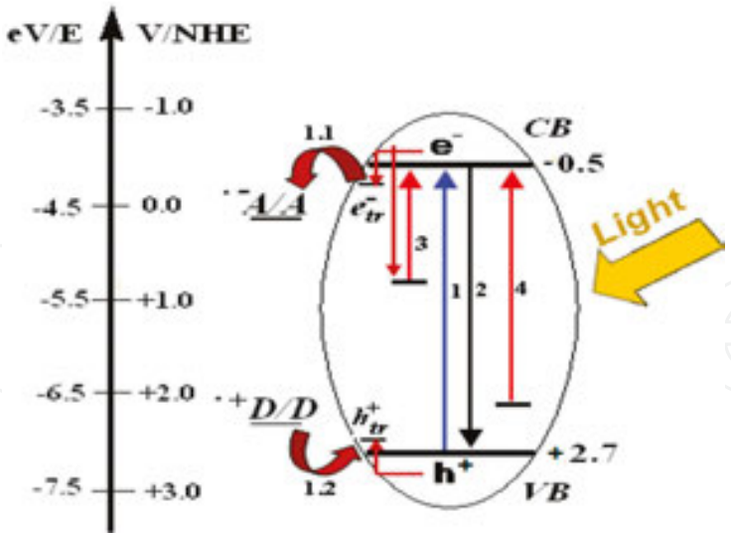


**Figure 1.** Schematic presentation of possible pathways after light absorption by doped titania particle.

defect state to the $TiO_2$ conduction band by photon with the lower energy (pathway 3). Inhibition of charge carrier recombination rate resulting in enhanced photoactivity is attributed to the transition metal ions doping of $TiO_2$. Visible-light illumination can generate a hole in the mid-gap level above the top of the VB for the N-doped $TiO_2$ (pathway 4).

The nitrogen-modified $TiO_2$ thin films exhibited photocurrents in the visible up to 700 nm as a result of occupied nitrogen-centered surface states above the valence band edge as noted in Ref. [41]. Moreover, the observed photocurrent under visible-light irradiation of N-doped $TiO_2$ in the presence of reducing agent strongly depend on the reaction mechanism of oxidation rather than on the redox potential of the whole acceptors [42]. Photo-electrochemical measurements showed that the visible-light photogenerated holes in $TiO_2$ modified by urea are able to oxidize formic acid comparing with ammonia modified one. An enhanced stabilization of the photogenerated hole against recombination with conduction band electrons for the former sample is explained [43]. In addition to the electrochemical investigations, preliminary computer simulations based on innovative cluster approaches demonstrated that nitrogen doping narrowed the optical bandgap of $TiO_2$ generating N(2p) states [44]. Density functional theory (DFT) was employed to demonstrate the interstitial nitrogen character within anatase $TiO_2$. No significant shift in the CB or VB of the $TiO_2$ was recognized. The energy bonding states associated below the valence band and anti-bonding states present above the valence band. The anti-bonding nitrogen orbital between the $TiO_2$ VB and CB is suggested to be responsible for the visible light absorption by acting as a stepping stone for excited electrons between conduction and valence bands [45].

Our investigation was directed to the synthesis of nitrogen-doped photocatalysts based on titania and/or mixed semiconductive oxides films and understanding the relationship between synthesis conditions, electronic structures, and photocatalytic activity. The influence of zirconium ions and its content as well as pulsed laser synthesis conditions on the efficiency of

nitrogen incorporation into titania structure that, in turn, determines the photocatalytic ability of the semiconductive materials are obtained.

## 2. Correlation of electronic structure, optical, structural, and photocatalytic properties of $TiO_2$-doped films

Pulsed laser deposition method used for the film synthesis allows obtaining high purity thin films of single or multicomponent materials [46]. ***PLD*** or ***laser ablation*** is a physical vapor deposition process based on the vaporization of condensed matter by means of photons [46–50]. A highly intense short-pulsed high-power laser beam (usually a ns UV one) is focused under vacuum or a working gas atmosphere on a piece of material (on a material specimen) called "target." If the laser fluence exceeds a specific threshold, one after one, each tiny quantity of ablated material by a laser pulse, is directed forward, in form of a plume, towards the deposition substrate, where the growing film is formed by recondensation [47–50]. Due to the high energetic species arriving on the substrate, the synthesized films are very adherent. The plasma plume plays a significant piston-like role, pushing and carrying the removed matter from the target to the substrate [49]. In the most common setup geometry, "on axis," the collector is placed parallel to the target, at a distance of some centimeters and, after being focused and transmitted by suitable optics, the laser pulses hit the target under 45°. The target is normally rotated in order to get a uniform ablation of its surface, avoiding drilling, thus obtaining a homogenous film. The collector, which is named usually "substrate," may be heated if a high degree of crystallinity or even epitaxy is of interest for the obtained coating. A schematic of PLD setup is given in **Figure 2**.

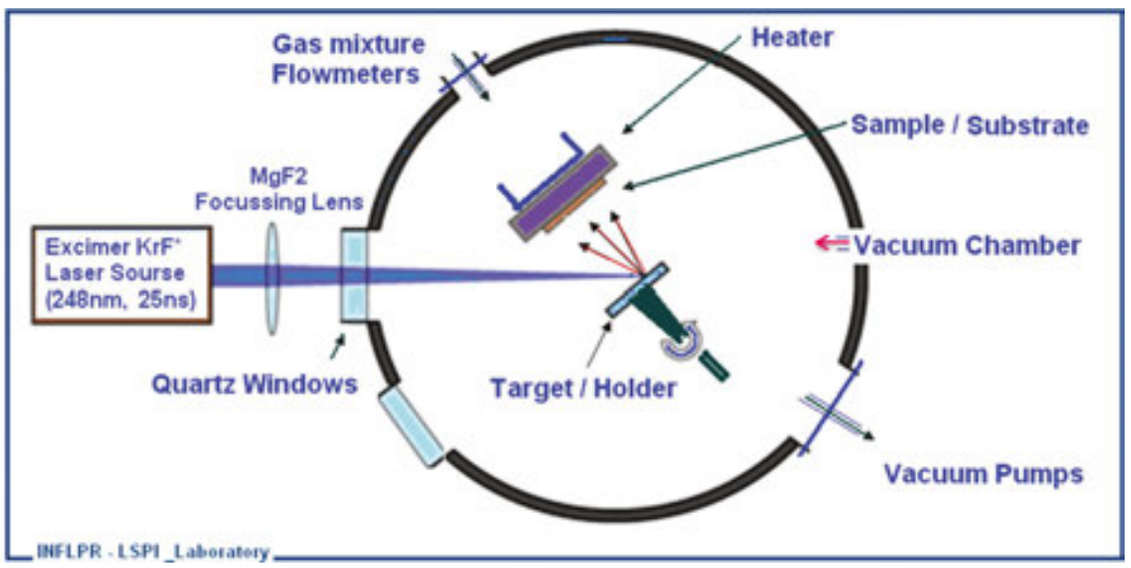


**Figure 2.** Schematic setup of a PLD system: The laser source is outside the deposition chamber, which is coupled to a vacuum system. Inside chamber, a classical "on axis" geometry is presented.

http://dx.doi.org/10.5772/62637

The PLD presents a series of advantages [47–50], among which we mention: almost any material or materials' combination may be congruently transferred as thin film on a suitable substrate after the identification of a selected deposition regime, a fine control of thickness is obtained by the number of the applied laser pulses (and the appropriate setting of various parameters), it is a clean, non-contaminating method, also allowing for an easy doping or multilayer structures. These and others made PLD a tool of remarkable performance, versatility, and simplicity for the growth of various types of thin films: complex oxides, high-temperature superconducting, protective or ultrahard coatings, polymer or organic thin films [50–52].

| $ZrO_2$% in $TiO_2$ | Ratio of gases | Sample code | P, Pa | t, °C | $E_{bg}$, eV |
|---|---|---|---|---|---|
| 0 | $O_2$ | **TiO/20** | 20 | 450 | 3.3 |
| 0 | $N_2$:$O_2$ = 1:1 | **TiNO/10** | 10 | 450 | 2.8 |
| 0 | $N_2$ | **TiN/20** | 20 | 450 | 2.6 |
| 0 | $CH_4$ | **TiC/5** | 5 | 450 | – |
| 0 | $N_2$:$CH_4$ = 5:1 | **TiN5C1/100** | 100 | 450 | 3.3 |
| 0 | $N_2$:$CH_4$ = 5:1 | **TiN5C1/3** | 3 | 450 | – |
| 2.5 | $O_2$ | **2.5ZrTiO/100** | 100 | 450 | 3.3 |
| 5 | $O_2$ | **5ZrTiO/100** | 100 | 450 | 3.4 |
| 10 | $O_2$ | **10ZrTiO/100** | 100 | 450 | 3.5 |
| 2.5 | $N_2$:$CH_4$ = 9:1 | **2.5ZrTiN9C1/100** | 100 | 450 | 3.0 |
| 5 | $N_2$:$CH_4$ = 9:1 | **5ZrTiN9C1/100** | 100 | 450 | 2.9 |
| 2.5 | $N_2$:$CH_4$ = 5:1 | **2.5ZrTiN5C1/100** | 100 | 450 | 3.4 |
| 5 | $N_2$:$CH_4$ = 5:1 | **5ZrTiN5C1/100** | 100 | 450 | 3.3 |
| 10 | $N_2$:$CH_4$ = 5:1 | **10ZrTiN5C1/100** | 100 | 450 | 3.1 |
| 50 | $N_2$:$O_2$ = 1:1 | **50ZrTiN1O1/5** | 5 | 600 | 3.5 |
| 50 | $O_2$ | **50ZrTiO/10** | 10 | 600 | 3.7 |
| 50 | $N_2$ | **50ZrTiN/10** | 10 | 600 | 3.0 |
| 50 | $CH_4$ | **50ZrTiC/10** | 10 | 600 | 3.2 |
| 50 | $N_2$:$CH_4$ = 10:1 | **50ZrTiN10C1/3** | 3 | 600 | – |
| 50 | $CH_4$ | **50ZrTiC/5** | 5 | 600 | – |
| 50 | $N_2$:$CH_4$ = 5:1 | **50ZrTiN5C1/10** | 10 | 600 | 3.6 |

**Table 1.** PLD conditions and bandgap values of $TiO_2$-based films.

PLD experiments were performed using a KrF* laser source (COMPexPro 205 Coherent, $\tau_{FWHM} \leq 25$ ns). Pristine $TiO_2$ or $ZrO_2$-mixed $TiO_2$ targets with different content of zirconium oxide were laser ablated to grow coatings on glass plates. The films were synthesized at substrate temperatures of 450 or 600°C. The samples were deposited at different pressure of pure oxygen, nitrogen, methane, and mixed $N_2$:$CH_4$ atmosphere with 1:1, 5:1, 9:1, and 10:1 ratios.

Photocatalytic activity of the films was assessed via dichromate ions reduction reaction. The film was immersed in 15 ml of an aqueous solution of potassium dichromate (in all experiments, the initial concentration of dichromate ions was $2*10^{-4}$ M) and the reducing agent (disodium salt of ethylenediaminetetraacetic acid) in the molar ratio 1:1 adjusted to pH ≥ 2 by perchloric acid. The mass of the films was found to be 0.40 ± 0.02 mg (the concentration of the catalyst in aqueous solution of redox couple was $2.7 \times 10^{-2}$ g/L, 37 times lower than usually used suspension 1 g/L). The reaction temperature was kept constant (25°C) during the experimental procedure. The change of Cr(VI) ions concentration was monitored with a Lambda 35 UV–Vis spectrophotometer (PerkinElmer) every 20 min. The film was immersed in the solution until complete adsorption in the dark occurred and then irradiated by 1000 W middle-pressure mercury lamp for 120 min. The distance lamp reactor was set at 90 cm. Two blank experiments were carried out: the catalytic reduction of dichromate ions (dark condition) and photoreduction reaction (a bare glass was used instead of film). The conversion percentage of every photocatalytic run is given after subtraction of the corresponding value of the last blank. For testing the visible-light sensitivity, a filter transmitting light with $\lambda > 380$ nm was introduced in the photocatalytic setup.

The sample codes that will appear over the chapter can be easily understand as ***x(Zr)TiYy(Zz)/P***, where ***x*** is the $ZrO_2$ percentage, ***(Zr)Ti*** is a target composition, ***Y*** and ***Z*** mean gas atmosphere (***O*** is $O_2$, ***N*** is $N_2$, ***C*** is $CH_4$), ***y*** and ***z*** are the ratio of ***Y*** and ***Z***, ***P*** is the gas pressure during PLD procedure. The synthesis conditions and the measured value of bandgap energy ($E_{bg}$) are collected in **Table 1**.

### 2.1. Nitrogen-doped $TiO_2$ films

Pulsed laser synthesis of $TiO_2$ films in oxygen, nitrogen, methane and their mixtures was performed (**Table 1**) [53]. Excluding the UV part of spectrum by cut-of-filter, the films obtained at different atmospheres exhibited the visible light absorption (**Figure 3**). Compared to bare $TiO_2$, nonmetal-doped films show a change in optical absorption that was originally associated to a bandgap narrowing. Comparing the values of bandgap energy calculated by extrapolating the linear parts of the $(\alpha h\nu)^{1/2} \sim f(h\nu)$ curves, that is assuming an indirect electronic transition (Table 1), the decrease in its values for the doped samples is obvious proving that the electronic structure of a photocatalyst affects its optical absorption. The sharp decrease of $E_{bg}$ was demonstrated when pure dinitrogen or the mixture of dinitrogen and oxygen has been applied.

http://dx.doi.org/10.5772/62637



**Figure 3.** Absorption spectra of TiO (1), TiN (2), TiN5C1 (3), TiNO (4), and cut-of-filter (dashed line).

As revealed by X-ray diffraction (XRD) spectra (**Figure 4**), anatase phase formation has been obtained for all films excepting TiC/5. Moreover, the samples TiNO/10 and TiO/20 present a preferential texture along the <004> plane. On the other hand, the peaks at 37.80°, 43.30°, and 62.80° visible in the diffractogram of the $TiO_2$ film deposited in $CH_4$ (TiC/5 film) could be related to <004>, <002>, and <202> planes of TiO phase indicating the formation of a sub-stoichiometric compound [53] or even Ti crystalline phase [29, 54, 55]. It is obvious that pure methane used in PLD prevents anatase formation providing oxygen atoms deficiency.



**Figure 4.** XRD spectra of $TiO_2$ films deposited at 450°C in oxygen, nitrogen, methane, and mixture of nitrogen and oxygen (*—anatase phase and #—TiO or Ti phase). Reproduced with permission from [53].

Intensity belonging to substitutional N*s* (N–Ti) lines at 395.2 and 395.8 eV for ***TiYy(Zz)/P*** is varied as clearly seen from **Figure 5** and **Table 1**. In addition, the appearance of the line at 397.8 and 398.1 eV accompanied by characteristic lines in the O*1s* and Ti*2p* spectra (not shown here) reveals a more complex structure of nitrogen in the doped $TiO_2$ films. The peak at *BE* ~ 457.5 eV in the Ti*2p* XPS spectrum of this film can be attributed to either the Ti atoms in the N–Ti–O linkages or Ti species interacting with $V_O$, whose formation is highly favored in the oxygen-poor conditions (**Table 2**) [57].

**Figure 5.** XPS spectra of N1s binding energy for samples ***TiNO/10*** (a) and ***TiN/20*** (b) adopted from [9] and ***TiN5C1/100*** (c) and ***TiN5C1/3*** (d). Adapted with permission from [56].

Replacing dinitrogen or the mixture of dinitrogen/oxygen by the mixture of dinitrogen/methane leads to the change not only the line intensities but also some peaks position. Quite surprisingly, the intensity of N1s peak of $N_s$ is sharply raised and reached ca. 90% for ***TiN5C1/3***. It points that no other nitrogen contained species are present in the lattice structure of titania for this materials. A new additional peak of $Ti2p_{3/2}$ region at lower BE (456.3 eV) is observed for ***TiN5C1/3***. Similarly, the $Ti2p_{3/2}$ lines corresponded to 455.6 and 456.9 eV appeared with increasing nitridation temperature leading to the formation of TiN phase as proven by XRD [29]. Taking into account that the peak at 456.3 eV is assigned by the published literature to TiN phase [30], it could be suggested the deeper nitrogen doping into titania at the low pressure (N–Ti–N and the dative-bonded N atoms). Thus, the deposition atmosphere and pressure have strong influence on the efficiency of $N_s$ and $N_i$ atoms incorporation.

| *BE*, eV | *TiNO/10* | *TiN/20* | *TiN5C1/100* | *TiN5C1/3* |
|---|---|---|---|---|
| | I, % | | | |
| *N1s* | | | | |
| 395.2 | – | 26.4 | – | – |
| 395.8 | 25.2 | – | 9.7 | 90.1 |
| 397.8 | – | – | 27.4 | – |
| 398.1 | – | 7.3 | – | – |
| 399.1 | 12.9 | 33.2 | 39.6 | 5.6 |
| 400.3 | 61.9 | 18.0 | – | – |
| 400.8 | – | – | 23.3 | 4.3 |
| 409.2 | – | 15.1 | – | – |
| $Ti2p_{3/2}$ | | | | |
| 456.3 | – | – | – | 15.3 |
| 457.5 | 2.6 | 16.8 | 24.4 | 20.3 |
| 458.1 | – | – | 60.6 | 48.1 |
| 458.3 | 62.9 | 67.9 | – | – |
| 458.8 | 34.5 | 15.3 | 15.0 | 16.3 |

**Table 2.** N1s and $Ti2p_{3/2}$ binding energy values and their relative intensity.

Comparing the bandgap energy values of ***TiN/20*** (2.6 eV), ***TiNO/10*** (2.8 eV), and ***TiN5C1/100*** (3.3 eV) with their intensity of $N_s$ peak 26.4, 25.2, and 9.7, respectively, the bandgap narrowing of anatase could result in the incorporation of substituted nitrogen.

| Sample | UV, % | vis, % |
|---|---|---|
| **TiC/5** | 15 | 3 |
| **TiO/20** | 24 | 3 |
| **TiNO/10** | – | 3 |
| **TiN/20** | – | 9 |
| **TiN5C1/100** | 25 | 9 |
| **TiN5C1/3** | – | 1 |

**Table 3.** Conversion percentage of dichromate ions after 120 min under UV and visible light.

The catalytic response under UV light exposure was observed for ***TiC/5***, ***TiO/20,*** and ***TiN5C1/100*** samples (**Table 3**). ***TiNO/10*** and ***TiN/20*** films were completely inactive under UV light, while the activity of ***TiN5C1/100*** is comparable with pure $TiO_2$ (***TiO/20***). The low activity of former N-doped materials could be explained by the nitrogen-induced levels formation in

the banggap of $TiO_2$, acting as recombination centers for charge carriers under irradiation with UV light. ***TiN/20*** and ***TiN5C1/100*** exhibited an identical level of photocatalytic conversion under visible light, while the relative intensities of $N_s$ (26.4 and 9.7 for TiN/20 and TiN5C1/100, respectively) and $N_i$ (7.3 and 27.4 for TiN/20 and TiN5C1/100, respectively) are different for these samples. No photocatalytic activity in the presence of TiN5C1/3 is observed.

## 2.2. Nitrogen-doped $ZrO_2/TiO_2$ films

### *2.2.1. Low content of $ZrO_2$ in the target*

Incorporation of transition metal oxides into titania improved the photocatalytic activity due to the mutual action of metal ions and anatase resulting in increased specific surface area, surface acidity, and changed photo-electrochemical properties. Coupling of two semiconductors is useful to achieve a more efficient separation of photogenerated electron–hole pair that led to the improvement of the photoactivity. It is found that the photocatalytic activity depends on the phase composition and crystalline size that modify the $TiO_2$ bandgap [11]. Zirconium incorporation into $TiO_2$ lattice by sol–gel synthesis was achieved with the formation of $Ti_{1-x}Zr_xO_2$ solid solution for the film with a Zr content up to 10 mol% as evidenced by XRD and XPS. It was demonstrated that the formation of Zr–O–Ti bonds has an influence on the thermal stability during sintering of the mesoporous structure of the films, surface texture, and optical properties as well as in the changes of number of surface active sites for nanocomposite films [10, 58].

Pulsed laser-deposited (2.5, 5, and 10%) $ZrO_2/TiO_2$ thin films were synthesized under various gas atmospheres (see Table 1). We inferred the characteristic $E_{bg}$ values for pure titania and zirconia of 3.3 and 4.2 eV. All nonmetal-doped films showed more intensive absorption extending into the visible-light region comparing ***xZrTiO/100***. A shift to the longer wavelength from lower to higher contents of $ZrO_2$ results in decrease of bandgap energy, as oppositely observed for the samples synthesized in $O_2$. The bandgap values of the films synthesized in a gas atmosphere with a higher ratio of $N_2$ to $CH_4$ (9:1) are lowered when increasing zirconia content.

For films synthesized at 3 Pa, the calculation of $E_{bg}$ was impossible because of the strong absorption in the visible region (**Figure 6** inset) [56]. Similar broad absorption was reported for N-doped $TiO_2$ after the nitridation by ammonia at 650°C or above and explained by the metallic property of samples as indicated by the XRD and transmission electron microscopy (TEM) result [29].

The N1s line at 395.8 eV attributed to $N_s$ is present for all nonmetal-doped samples. The XPS spectra of ***2.5ZrTiN9C1/100*** and ***2.5ZrTiN5C1/100*** films showed almost the same relative intensity of $N_s$ lines as ***TiN5C1/100*** (**Figures 5c** and **7b**, **d**) and **Tables 2** and **4**). On the other hand, the increased intensity of $N_s$ lines is fixed for the samples containing 5% $ZrO_2$, especially for the film synthesized at higher ratio of $N_2$ to $CH_4$ (***5ZrTiN9C1/100***). It shows that the higher the dinitrogen content in the gas mixture, the more substitutional nitrogen is incorporated in the semiconductive structure. Comparing the intensity of N1s line at 395.8 eV of all samples

http://dx.doi.org/10.5772/62637

synthesized at 100 Pa, it is evident that highest peak intensity (~43%) corresponds to the sample with the largest content (10%) of zirconia, while the lowest intensity at 397.8 eV is observed.

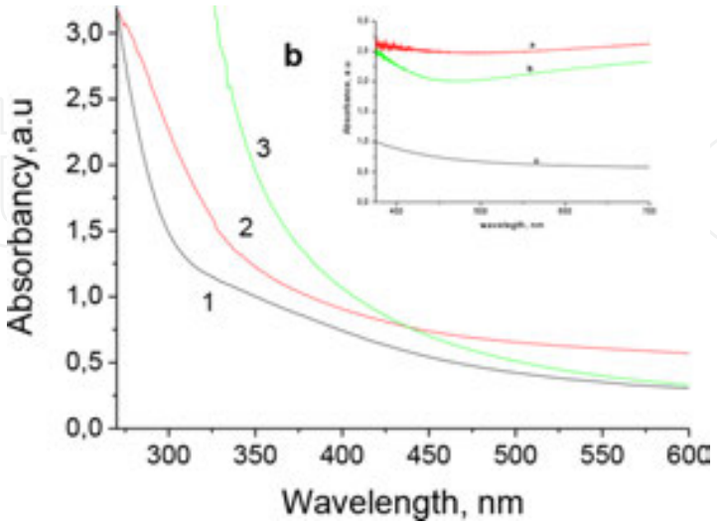


**Figure 6.** Absorption spectra of ***2.5ZrTiN5C1/100*** (1), ***5ZrTiN5C1/100*** (2), and ***10ZrTiN5C1/100*** (3). Inset: samples ***5ZrTiN5C1/3***—a, ***5ZrTiN9C1/3***—b, ***5ZrTiN5C1/100***—c. Reproduced with permission from [56].

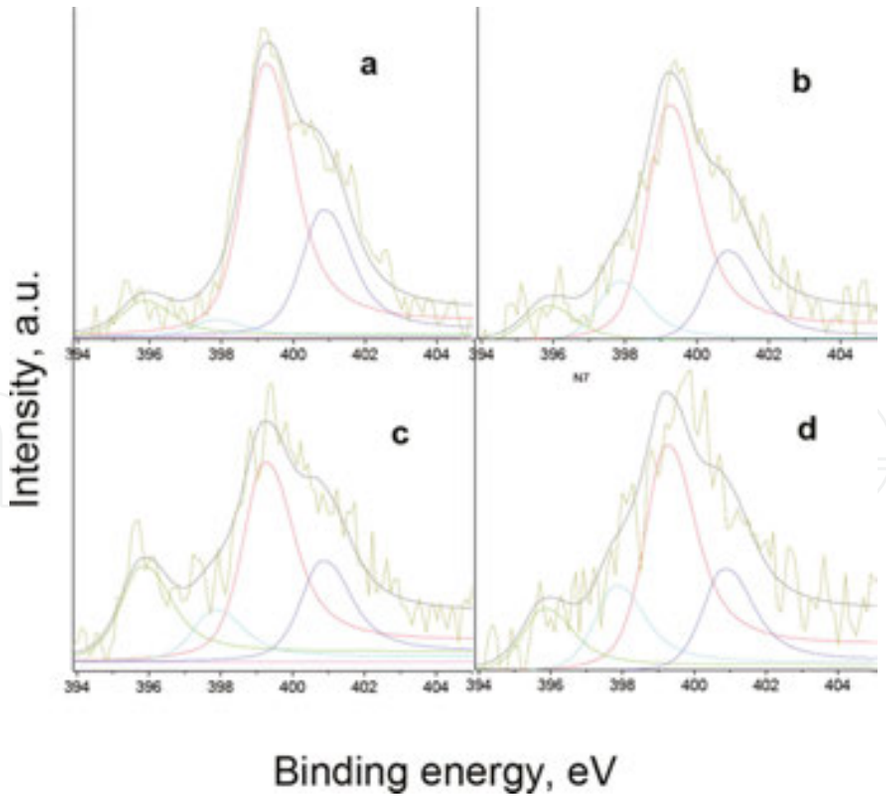


**Figure 7.** XPS spectra of N1s binding energy for ***2.5ZrTiN9C1/100*** (a), ***2.5ZrTiN5C1/100*** (b), ***5ZrTiN9C1/100*** (c), and ***5ZrTiN5C1/100*** (d) samples. Reproduced with permission from [56].

| *BE, eV* | *2.5ZrTiN9C1/100* | *2.5ZrTiN5C1/100* | *5ZrTiN9C1/100* | *5ZrTiN5C1/100* |
|---|---|---|---|---|
| | | | **I, %** | |
| *N1s* | | | | |
| 395.8 | | | | |
| 397.8 | 3.8 | 14.4 | 11.6 | 18.1 |
| 399.2 | 60.3 | 55.5 | 44.5 | 47.0 |
| 400.8 | 27.9 | 21.4 | 22.5 | 21.5 |
| $Ti2p_{3/2}$ | | | | |
| 457.5 | 3.2 | 7.2 | 11.2 | 5.1 |
| 458.3 | 68.3 | 57.4 | 72.9 | 63.5 |
| 458.8 | 28.5 | 35.4 | 15.9 | 31.4 |

**Table 4.** N1s and $Ti2p_{3/2}$ binding energy values and their relative intensity.

Analogous to ***TiN5C1/3,*** $N_s$ peak for ***10ZrTiN5C1/3*** films contains the single high-intensity N1s line at 395.7 eV. No other deconvoluted peaks were found (**Figure 8**; **Table 5**). Thus, an incorporation of substitutional nitrogen ions without any other forms can be achieved by carrying the synthesis at 3 Pa pressure.

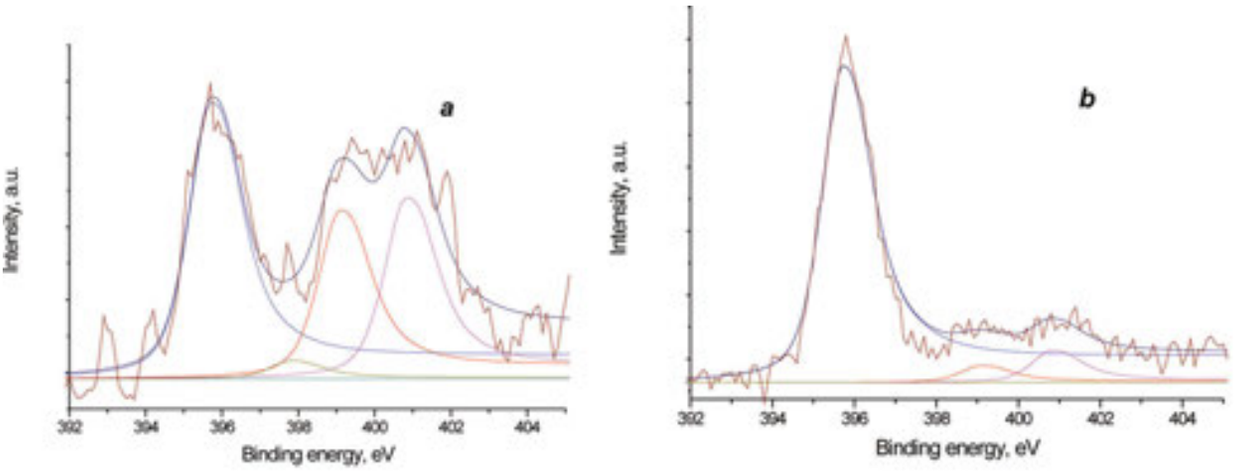


**Figure 8.** XPS spectra of N1s binding energy for ***10ZrTiN5C1/100*** (a) and ***10ZrTiN5C1/3*** samples (b).

Such effective nitrogen incorporation in oxide matrix can be the effect of an interaction between carbon (and/or hydrogen) and laser ablated oxygen atoms forming $CO_2$ during PLD that leads to the oxygen deficiency and the formation of nonstoichiometric $TiO_{2-x}N_x$ structure. This can be confirmed by the lower ratio (1.6) of $O_{Ti}1s/Ti2p$ for samples synthesized at 3 Pa in comparison with pristine $TiO_2$ where this ratio equals 2 [56].

http://dx.doi.org/10.5772/62637

| ***BE*, eV** | ***10ZrTiN5C1/100*** | ***10ZrTiN5C1/3*** |
|---|---|---|
| | **(a)** | **(b)** |
| | **I, %** | |
| *N1s* | | |
| 395.7 | 43.2 | 86.8 |
| 397.8 | 2.8 | – |
| 399.1 | 26.2 | 4.6 |
| 400.8 | 27.9 | 8.7 |
| $Ti2p_{3/2}$ | | |
| 456.3 | – | 8.1 |
| 457.5 | 21.0 | 37.2 |
| 458.1 | 72.80 | 47.1 |
| 458.8 | 6.24 | 7.6 |

**Table 5.** Relative intensity of N1s and $Ti2p_{3/2}$ binding energy.

A significant intensity of peak at 457.5 eV assigned to the Ti–N bonds was observed for ***10ZrTiN5C1/100*** and ***10ZrTiN5C1/3***, assuming also the presence of $Ti^{3+}$ states. According to the literature [59], such titanium species have oxidation states between +3 and +4. Moreover, the appearance of additional $Ti2p_{3/2}$ peaks with lower BE similar to ***TiN5C1/3*** (Section 2.1) is assigned to the change of surrounding titanium, where more oxygen atoms are substituted by nitrogen. The $Zr3_{d5/2}$ line ($E_{bg}$ = 182.3 eV) was recorded for all zirconia-containing samples, meaning the formation of $Zr^{4+}$ ions surrounded by $O^{2-}$ ions [10]. No signal pointing on the formation of Ti–O–Zr bonds was obtained (not shown here).

Additionally, the ratio of N1s line at 395.8 eV to $Ti2p_{3/2}$ line at 457.5 eV corresponds as 1:2 and 2:1 for ***TiN5C1/100*** and ***10ZrTiN5C1/100***, respectively. It is supposed that the distortion of $Ti^{4+}O_2$ lattice with the advent of $Ti^{3+}$ states occurs due to larger size of zirconium ions ($R_{Zr4+}$ = 0.720 Å vs. $R_{Ti4+}$ = 0.650 Å). The relatively high stability of $Ti^{3+}$ states of the tested samples is associated to the presence of $Zr^{4+}$ ions. Note that the non-equilibrium character of the PLD process is favorable to the generation of strains in the lattice. XPS data pointed to the correlation between zirconium contents and ratio of number of nitrogen atoms linked in Ti–N bonds to the number of $Ti^{3+}$ states as well as the relative contents of N1s at 395.8 eV. This can be indicative for the formation of Ti–N fragments in the coordination sphere of $Ti^{3+}$ ions. In other words, the $N_s$ states (395.8 eV) responsible for photocatalytic activity of doped samples could be also connected with $Ti^{3+}$ states of $Ti^{4+}O_2$ lattice.

Certainly, the non-doped $ZrO_2/TiO_2$ films (columns 7, 8, and 9 in **Figure 9**) exhibit much lower activity under both UV and visible light compared to nitrogen-doped synthesized at 100 Pa. The highest yield under both UV (51% reduced ions) and visible light (14%) was demonstrated by ***10ZrTiN5C1/100***. The activity of this film is twice higher than ***TiO/20*** and ***TiN5C1/100*** under UV light and 1.5 times higher comparing with ***TiN/20*** and ***TiN5C1/100*** under visible light. We

have shown that the conversion percentage under UV light is strongly correlated with the contribution of N1s at 395.8 eV which in turn depends on the zirconia content (Tables 4 and 5). Hence, the photocatalytic activity strongly depends on the efficiency of substitutional nitrogen incorporation inside titania matrix that is, in turn, affected by zirconia content and the gas ratio used during PLD synthesis.

**Figure 9.** Conversion of dichromate ions after 120 min under visible (a) and UV (b) light: 1—***TiN5C1/100***; 2—***2.5ZrTiN5C1/100***; 3—***5ZrTiN5C1/100***; 4—***10ZrTiN5C1/100***; 5—***2.5ZrTiN9C1/100***; 6—***5ZrTiN9C1/100***; 7—***2.5ZrTi/100***; 8—***5ZrTi/100***; 9—***10ZrTi/100***.

It must be emphasized that all films obtained at lowest pressure are completely inactive under both UV and visible-light irradiation (not shown here). In order to understand in depth this

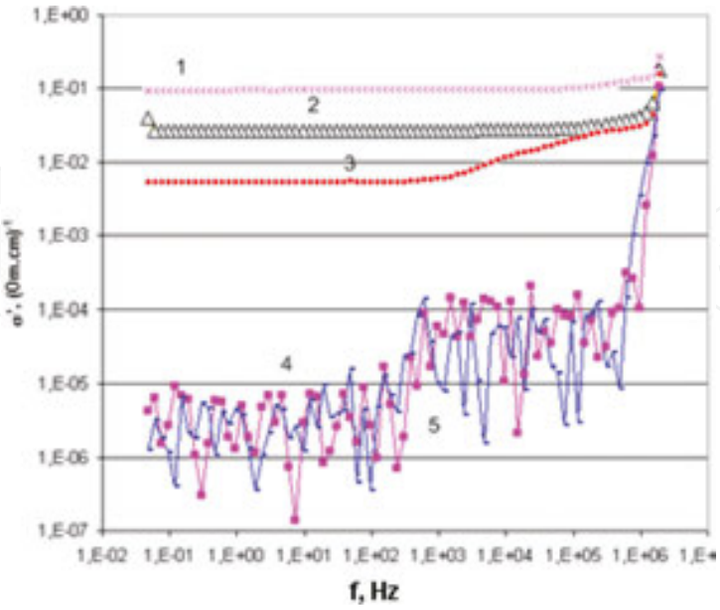


**Figure 10.** Electrical conductivity of ***10ZrTiN5C1/X***: 3 (1), 6 (2), 10 (3), 50 (4), and 100 Pa (5).

http://dx.doi.org/10.5772/62637

phenomenon, the electrical conductivity (**Figure 10**) measurements were performed. The samples obtained in the range of (3–10) Pa are black colored (**Figure 11**) and exhibit the electrical conductivity pointing on the appearance of oxygen vacancies, which results in metallic character of these materials. The formation of nonstoichiometric $TiO_{2-x}N_x$ containing in excess of Ti–N bonds exhibiting a low semiconductive behavior is concluded.

Moreover, no electrical conductivity (**Figure 10**, curves 4 and 5) was observed for the samples obtained at 50 and 100 Pa providing their semiconductive behavior. This indicates that anatase in conjunction with a certain numbers of Ti–N bonds is beneficial on the effective photocatalytic transformations.

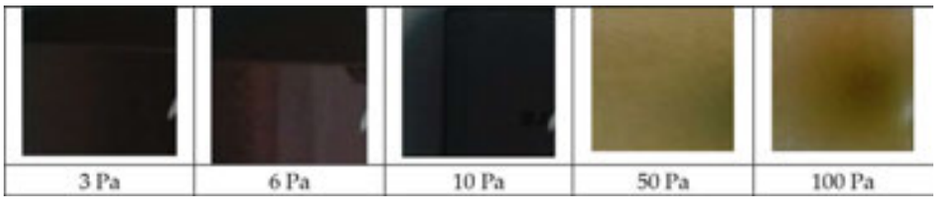


**Figure 11.** Images of ***10ZrTiN5C1/X*** obtained under different gas pressures.

As seen from **Figure 11**, the level of nitrogen incorporation strongly affects the optical properties of the films which turned from black to dark yellow color.

### *2.2.2. High weight content of $ZrO_2$ in the sample*

The next series of the films used in our investigation was based on the mixed titania–zirconia films with the component ratio 50:50 wt%. The synthesis conditions are detailed in **Table 1**.

**Figure 12.** Absorption spectra of ***50ZrTiO/10*** (1), ***50ZrTiN1O1/5*** (2), ***50ZrTiN5C1/10*** (3), and ***50ZrTiN/10*** (4) films.

$TiO_2/ZrO_2$ films prepared in ambient $N_2$ and/or $CH_4$ atmosphere had different absorption spectra. The shift of the absorption band edge to the red region of the spectra with the increase of $N_2$ content in the gas mixtures was observed (**Figure 12**). The influence of the doping agent nature and its content was observed in the variation of bandgap energy values (**Table 1**).

Similar to the bandgap values of low zirconia content films (Section 2.2.1), $E_{bg}$ values correlate with dinitrogen content in the gas mixture and applied pressure. For non-doped $ZrO_2/TiO_2$ (***50ZrTiO/10***), the bandgap energy value is higher (3.7 eV) than for anatase, pointing on the presence of wide bandgap semiconductor as zirconia. In particular, the $E_{bg}$ values are decreased with the increase of dinitrogen content in a gas mixture, reaching 3.0 eV for ***50ZrTiN/10***. On the other hand, for the doped composite samples ***50ZrTiN10C1/3*** and ***50ZrTiC/5***, the calculation of $E_{bg}$ was impossible because of the strong absorption in the visible region.

Unexpectedly, no crystallization of titania but incipient crystallization corresponding to the (101) line of $ZrO_2$ were confirmed by XRD investigation (not shown here) [60]. It can be explained by the existence of undetectable very small $TiO_2$ particles or by the excess of $ZrO_2$ in the film matrix inhibiting the titania crystallization.

**Figure 13.** XPS spectra of N1s energy for the samples ***50ZrTiN/10*** (a), ***50ZrTiN5C1/10*** (b), ***50ZrTiN10C1/3*** (c).

The sample synthesized at the high content of $N_2$ in the gas mixture (***50ZrTiN10C1/3***) contains the most prominent peaks of $Ti2p_{3/2}$ at 457.5 eV and N1s at 395.8 eV (**Figure 13**; **Table 6**), indicating the effective $N_s$ incorporation at low pressure similar to low zirconia content films (Section 2.2.1). Existence of other nitrogen species (400 eV) could be explained by high content of zirconia that caused the distortion of the crystalline lattice and easier incorporation of other N species. Almost equal intensity of the peaks at 395.8 and 400.0 eV was observed for sample deposited in pure $N_2$. The $Ti2p_{3/2}$ signal at 457.5 eV was weaker for sample obtained in pure $N_2$ than in 5:1 $N_2$:$CH_4$ at 10 Pa. The binding energy of $Zr3d_{5/2}$ peak for all samples (182.3 eV) corresponded to $Zr^{4+}$ species in $ZrO_2$.

| *BE, eV* | *50ZrTiN/10* **(a)** | *50ZrTiC/5* **(b)** | *50ZrTiN5C1/10* **(c)** | *50ZrTiN10C1/3* **(d)** |
|---|---|---|---|---|
| | **I,%** | | | |
| ***N1s*** | | | | |
| 395.8 | 42.5 | – | 27.6 | 67.6 |
| 400.0 | 57.5 | 100 | 68.5 | 32.4 |
| ***Ti2p*$_{3/2}$** | | | | |
| 457.5 | 7.5 | – | 8.1 | 23.5 |
| 458.3 | 36.9 | 9.0 | 31.7 | 27.8 |
| | 55.6 | 91.0 | 60.2 | |

**Table 6.** Relative intensity of N1s and Ti2$p_{3/2}$ binding energy from Figure 13.

*All the films were inert under UV and visible-light irradiation showing an activity similar to that of blank sample.* The photocatalytic performance of ***50ZrTiN10C1/3*** film was comparable to $TiO_2$ one under UV light. The highest activity for this series of films was reached for the structure with the largest number of $N_s$ [60]. As clearly seen, no favorable effect of half doping level of $ZrO_2$ in titania was recognized as a result of the low crystallization degree of anatase, while the synthesis conditions for the effective nitrogen substitution were chosen.

## 3. Conclusions

In summary, an appropriate selection of gas mixture, pressure, and temperature during PLD synthesis is identified for the optimum photocatalytic activity of semiconductive materials. The highest photocatalytic conversion yields in the dichromate ions reduction are obtained for nitrogen-doped 10% $ZrO_2/TiO_2$ synthesized in $N_2$:$CH_4$ = 5:1 at 100 Pa and at 450°C under both UV and visible light. This is the result of effective nitrogen atom substitution into titania lattice as confirmed by N1s XPS line at 395.8 eV. When the films were synthesized at low pressure of 3 Pa, the only Ns peak with the binding energy 395.8 eV was observed and photocatalytically inactive nonstoichiometric $TiO_{2-x}N_x$ structures were deposited. The absence of semiconductive properties of the films obtained at the low pressures is a direct evidence of no anatase formation and, respectively, their photocatalytic performance remained at the level of blank experiments. It can be suggested that carbon and hydrogen radicals/atoms forming as a result of laser action react with oxygen species causing the subsequent oxygen substitution by nitrogen atoms. This mechanism is supported by the XPS evidence, according to which the intensity of N–Ti peak at 395.9 eV is lower for the samples synthesized in a pure $N_2$ atmosphere. Thus, the effective incorporation of substitutional nitrogen in oxide matrix can be caused by a direct interaction of carbon or hydrogen atom with oxygen species during PLD resulting in an oxygen deficient lattice, taking into account that pure methane used in PLD prevents anatase formation providing oxygen atoms deficiency. At high pressure, a number of collisions between C or H species and ablated oxygen atoms are less probable owing to the screening effect of other atoms/species (**Figure 14**a). When pressure is decreased, the deposition rate is enhanced in

addition to much higher probability for carbon/oxygen and hydrogen/oxygen interactions (**Figure 14**b). This can result in the higher efficiency of Ti–N as compared with Ti–O fragments formation.

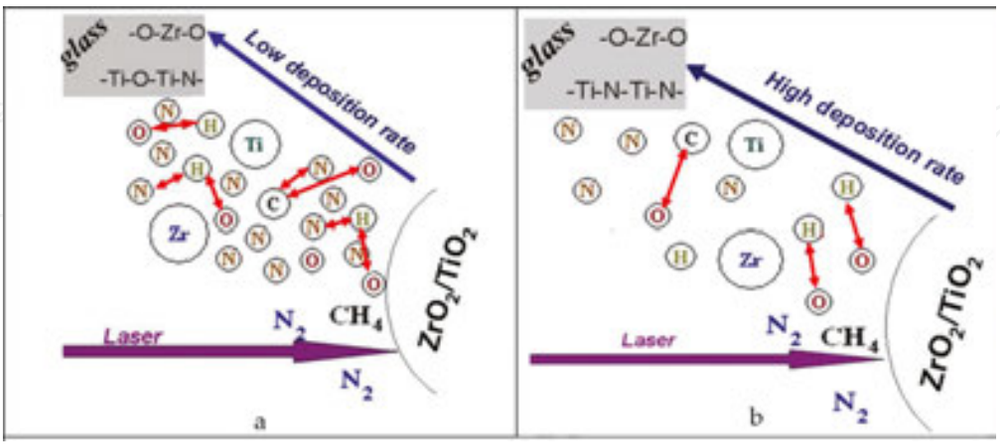


**Figure 14.** Schematic representation of pulse laser deposition in a mixture of $N_2/CH_4$ at 100 Pa (a) and 3 Pa (b).

As seen from **Figure 15**, the percentage of reduced dichromate ions under UV light is correlated with the contributions of N1s at 395.8 eV which is in turn dependent on the zirconia content. The ratio of line intensities of N1s at 395.8 eV to $Ti2p_{3/2}$ at 457.5 eV is pointing to the large number of $O–Ti^{3+}–N$ bonds with the increase of $ZrO_2$ contents. It is obvious that photocatalytic activity under UV light strongly depends on the efficiency of substitutional nitrogen incorporation inside titania matrix. The high $ZrO_2$ content (50%) induces the deceleration of anatase crystallization rate leading to the activity decrease, while a much lower zirconia amount (2.5 and 5%) is still not enough to stimulate an appropriate quantity of substituted nitrogen embedded in titania matrix. The correlation between the zirconia content and the efficiency of substitutional N incorporation is established. The distortion of $Ti^{4+}O_2$ lattice with the advent

**Figure 15.** Influence of zirconia contents in ***(xZr)TiN5C1/100*** films on the photocatalytic conversion under UV (black column), ratio of N1s at 395.8 eV to Ti2p at 457.5 eV (red column) and N1s at 395.8 eV to total N1s (blue column). Reproduced with permission from [56].

http://dx.doi.org/10.5772/62637

of $Ti^{3+}$ states occurred due to the larger radius of zirconium ions ($R_{Zr4+}$ = 0.720 Å vs. $R_{Ti4+}$ = 0.650 Å). The relative high stability of $Ti^{3+}$ states is assigned to the presence of $Zr^{4+}$ ions.

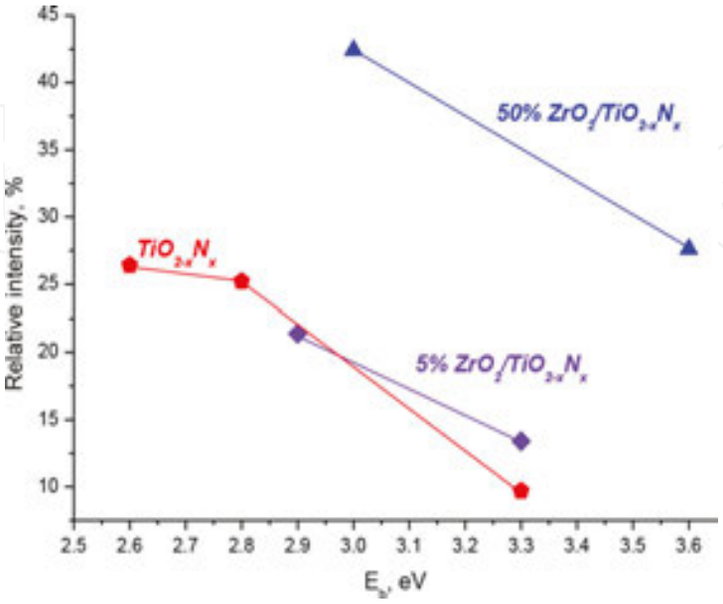


**Figure 16.** Dependence of bandgap energy of the semiconductive materials with the relative intensity of N1s XPS signal at 395.2–395.8 eV.

In general, the low photocatalytic efficiency is explained by the limited photo-excitation of electrons in the intragap localized states, the very low mobility of photogenerated holes [2], and the high recombination rate due to the creation of oxygen vacancies by doping [61]. Hence, the photoreactivity of doped $TiO_2$ appeared to be a complex function of the doping agent concentration, the energy level of doping agent within the $TiO_2$ lattice, their d electronic configurations, the distribution of doping agent, the electron donor concentrations, and light intensity.

The debates concerning the preferred N substitutional or interstitial sites which induce the highest photocatalytic action is still alive in the literature [62–64]. Our investigation suggests that the substitutional nitrogen (Ti–N) that belongs to XPS lines at 395.2–395.8 eV is basically responsible for the observed photoactivity. Additionally, it can be proved by the next two observations. (i) The peak at 397.8 eV has the negligible relative intensity (2.8%) for most active **10ZrTiN5C1/100,** and (ii) the peaks in the range of 398–401 eV are observed for the other samples with low reactivity. We also underline that $N_s$ species with 395.2–395.8 eV binding energy are responsible for bandgap narrowing or formation of intragap localized states of the doping agent within bandgap (**Fig. 16**). It is pointed that the bandgap energy values are sharply declined when the relative intensity of this XPS peaks is increased, while no dependence between 397.8 or 398–401 eV peaks and $E_{bg}$ is observed. PLD synthesis of $TiO_2$ films in $N_2/CH_4$ atmosphere not only leads to nitrogen incorporation but also to the formation of defects including oxygen vacancies and $Ti^{3+}$ states which are all contributing to light absorption.

## Acknowledgements

All authors acknowledge the collaboration between Romanian Academy and National Academy of Sciences of Ukraine. Romanian authors acknowledge with thanks the support of CNCS-UEFISCDI under the contract ID304/2011 and Core Programme 2016–2017 LAPLACE-IV.

## Author details

Oksana Linnik[1], Nataliia Chorna[1], Nataliia Smirnova[1], Anna Eremenko[1], Oleksandr Korduban[2], Nicolaie Stefan[3], Carmen Ristoscu[3], Gabriel Socol[3], Marimona Miroiu[3] and Ion N. Mihailescu[3*]

*Address all correspondence to: ion.mihailescu@inflpr.ro

1 Chuiko Institute of Surface Chemistry, National Academy of Science of Ukraine, Kyiv, Ukraine

2 Kurdyumov Institute of Metallophysics, National Academy of Sciences of Ukraine, Kyiv, Ukraine

3 National Institute for Lasers, Plasma and Radiation Physics, Magurele, Ilfov, Romania

## References

[1] Fujishima A., Rao TN, Tryk DA., Titanium dioxide photocatalysis. *J. Photochem. Photobiol. C: Photochem. Rev*. 2000; 1(1): 1–21.

[2] Hashimoto K., Irie H., Fujishima A., $TiO_2$ photocatalysis: a historical overview and future prospects. *Jpn. J. Appl. Phys*. 2005; 44: 8269–8285.

[3] Thompson TL, Yates JTJr, Surface science studies of the photoactivation of $TiO_2$ new photochemical processes. *Chem. Rev*. 2006; 106: 4428–4453.

[4] Fujishima A., Honda K., Electrochemical photolysis of water at a semiconductor electrode. *Nature*. 1972; 238(5358): 37–38.

[5] Frank SN, Bard AJ, Heterogeneous photocatalytic oxidation of cyanide ion in aqueous solutions at titanium dioxide powder. *J. Am. Chem. Soc*. 1977; 99(1): 303–304.

[6] Wang R., Hashimoto K., Fujishima A., Chikuni M., Kojima E., Kitamura A., Shimohigoshi M., Watanabe T., Light-induced amphiphilic surfaces. *Nature*. 1997; 388: 431–432.

[7] O'Regan B., Gratzel M., Low-cost, high-efficiency solar cell based on dye-sensitized colloidal $TiO_2$ films. *Nature* 1991; 353: 737–739.

[8] Fujishima A., Zhang X., Tryk D.A., $TiO_2$ photocatalysis and related surface phenomena. *Surf. Sci. Rep*. 2008; 63 (12): 515–582.

[9] Sakthivel S., Kisch H., Daylight photocatalysis by carbon-modified titanium dioxide. *Angew. Chem. Int. Ed*. 2003; 42 (40): 4908–4911.

[10] Gnatyuk Y., Smirnova N., Eremenko A., Ilyinl V., Design and photocatalytic activity of mesoporous $TiO_2$/Zr $O_2$ thin films, *Adsorp. Sci. Technol*. 2005; 23(6); 497–408.

[11] Smirnova N., Gnatyuk Y., Vityuk N., Linnik O., Eremenko A., Vorobets V., Kolbasov G., Nanosized $TiO_2$-based mixed oxide films: sol–gel synthesis, structure, electrochemical characteristics and photocatalytic activity. *Int. J. Mater. Eng*. 2013; 3(6): 124–135.

[12] Smirnova N., Vorobets V., Linnik O., Manuilov E., Kolbasov G., Photoelectrochemical and photocatalytic properties of mesoporous $TiO_2$ films modified with silver and gold nanoparticles. *Surf. Interface. Anal*. 2010; 42: 1205–1208.

[13] Linnik O., Smirnova N., Korduban O., Eremenko A., Gold nanoparticles into $Ti_{1-x}Zn_xO_2$ films: synthesis, structure and application. *Mater. Chem. Phys*. 2013; 142 (1): 318–324.

[14] Linnik O., Kisch H., On the mechanism of nitrogen photofixation at nanostructured iron titanate films. *Photochem. Photobiol. Sci*. 2006; 5: 938–942.

[15] Linnik O., Kisch H., Dinitrogen photofixation at ruthenium-modified titania films. *Mendeleev Commun*. 2008; 18(1): 10–11.

[16] Shestopal N., Linnik O., Smirnova N., Influence of metal and non-metal ions doping on the structural and photocatalytic properties of titania films. *Chem. Phys. Technol. Surf*. 2015; 6(2): 203–210.

[17] Sato S., Photocatalytic activity of $NO_x$-doped $TiO_2$ in the visible light region, *Chem. Phys. Lett*. 1986; 123: 126–128.

[18] Asahi R., Morikawa T., Ohwaki T., Aoki K., Taga Y., Visible-light photocatalysis in nitrogen-doped titanium dioxide. *Science*. 2001; 293: 269–271.

[19] Abadias G., Paumier F., Eyidi D., Guerin P., Girardeau T., Structure and properties of nitrogen-doped titanium dioxide thin films produced by reactive magnetron sputtering. *Surf. Interface. Anal*. 2010; 42: 970–973.

[20] Nakano Y., Morikawa T., Ohwaki T., Yaga Y., Deep-level optical spectroscopy investigation of N-doped $TiO_2$ films. *Appl. Phys. Lett*. 2005; 86: 132104.

[21] Li Jinlong, Xinxin M., Mingren S., Li X., Zhenlun S., Fabrication of nitrogen-doped mesoporous $TiO_2$ layer with higher visible photocatalytic activity by plasma-based ion implantation. *Thin. Solid. Films*. 2010; 519 (1): 101–105.

[22] Pore V., Heikkila M., Ritala M., Leskela M., Arev S., Atomic layer deposition of $TiO_{2-x}N_x$ thin films for photocatalytic applications. *J. Photochem. Photobiol. A Chem.* 2006; 177 (1); 68–75.

[23] Zhao L., Jiang Q., Lian J., Visible-light photocatalytic activity of nitrogen-doped $TiO_2$ thin film prepared by pulsed laser deposition. *Appl. Surf. Sci.* 2008; 254 (15): 4620–4625.

[24] Kafizas A., Crick C., Parkin IP, The combinatorial atmospheric pressure chemical vapour deposition (c APCVD) of a gradating substitutional/interstitial N-doped anatase $TiO_2$ thin-film; UVA and visible light photocatalytic activities. *J. Photochem. Photobiol. A: Chem.* 2010; 216 (2–3): 156–166.

[25] Irie H., Watanabe Y., Hashimoto K., Nitrogen-concentration dependence on photocatalytic activity of $TiO_{2-x}N_x$ powders. *J. Phys. Chem. B* 2003; 107(23): 5483–5486.

[26] Serpone N., Is the band gap of pristine $Tio_2$ narrowed by anion- and cation-doping of titanium dioxide in second-generation photocatalysts? *J. Phys. Chem. B* 2006; 110 (48): 24287–24293.

[27] Chen X., Wang X., Hou Y., Huang J., Wu L., Fu X., The effect of postnitridation annealing on the surface property and photocatalytic performance of N-doped Ti $O_2$ under visible light irradiation. *J. Catal.* 2008; 255 (1): 59–67.

[28] Mitoraj D., Kisch H., The nature of nitrogen-modified titanium dioxide photocatalysts active in visible light. *Angew. Chem. Int. Ed.* 2008; 47(51): 9975–9978.

[29] Zhang Z., Wang X., Long J., Gu Q., Ding Z., Fu X., Nitrogen-doped titanium dioxide visible light photocatalyst: spectroscopic identification of photoactive centers. *J. Catal.* 2010; 276 (2): 201–214.

[30] Saha NC, Tompkins HG, Titanium nitride oxidation chemistry: an x-ray photoelectron spectroscopy study. *J. Appl. Phys.* 1992; 72: 3072–3079.

[31] Nosaka Y., Matsushita M., Nishino J., Nosaka AY, Nitrogen-doped titanium dioxide photocatalysts for visible response prepared by using organic compounds. *Sci. Technol. Adv. Mater.* 2005; 6(2): 143–148.

[32] Cong Y., Zhang J., Chen F., Anpo M., Synthesis and characterization of nitrogen-doped $TiO_2$ nanophotocatalyst with high visible light activity. *J. Phys. Chem. C* 2007; 111 (19): 6976–6982.

[33] Beranek R., Kisch H., Tuning the optical and photoelectrochemical properties of surface-modified $TiO_2$. *Photochem. Photobiol. Sci.* 2008; 7: 40–48.

[34] Mitoraj D., Kisch H., On the mechanism of urea-induced titania modification. *Chem. Eur. J.* 2010; 16: 261–269.

[35] Napoli F., Chiesa M., Livraghi S., Giamello E., Agnoli S., Granozzi G., Pacchioni G., Di Valentin C., The nitrogen photoactive centre in N-doped titanium dioxide formed via

interaction of N atoms with the solid. Nature and energy level of the species. *Chem. Phys. Lett*. 2009; 477 (1–3): 135–138.

[36] Livraghi S., Giamello MRCE, Magnacca G., Paganini MC, Cappelletti G., Bianchi CL, Nitrogen-doped titanium dioxide active in photocatalytic reactions with visible light: a multi-technique characterization of differently prepared materials. *J. Phys. Chem. C* 2008; 112 (44): 17244–17252.

[37] György E., Pérez del Pino A., Serra P., Morenza JL, Depth profiling characterisation of the surface layer obtained by pulsed Nd:YAG laser irradiation of titanium in nitrogen. *Surf. Coat. Technol*. 2003; 173 (2–3): 265–270.

[38] Chen X., Burda C., Photoelectron spectroscopic investigation of nitrogen-doped titania nanoparticles. *J. Phys. Chem. B* 2004; 108 (40): 15446–15449.

[39] Diwald O., Thompson TL, Zubkov T., Goralski EGO, Walck SD, Yates JT, Photochemical activity of nitrogen-doped rutile $TiO_2$(110) in visible light. *J. Phys. Chem. B* 2004; 108 (19): 6004–6008.

[40] Reyes-Garcia EA, Sun Y., Reyes-Gil K., Raftery D., 15N solid state NMR and EPR characterization of N-doped $TiO_2$ photocatalysts. *J. Phys. Chem. C* 2007; 111 (6): 2738–2748.

[41] Beranek R., Kisch H., Surface-modified anodic $TiO_2$ films for visible light photocurrent response. *Electrochem. Commun*. 2007; 9 (4): 761–766.

[42] Nakamura R., Tanaka T., Nakato Y., Mechanism for visible light responses in anodic photocurrents at N-doped $TiO_2$ film electrodes. *J. Phys. Chem. B* 2004; 108 (30): 10617–10620.

[43] Mitoraj D., Berranek R., Kisch H., Mechanism of aerobic visible light formic acid oxidation catalyzed by poly(tri-s-triazine) modified titania. *Photochem. Photobiol. Sci*. 2010; 9: 31–38.

[44] Melhem H., Simon P., Wang J., Di Bin C., Ratier B., Leconte Y., Herlin-Boime N., Makowska-Janusik M., Kassiba A., BoucléJ., Direct photocurrent generation from nitrogen doped $TiO_2$ electrodes in solid-state dye-sensitized solar cells: towards optically-active metal oxides for PV applications. *Solar Energy Mater. Solar Cells*. 2012; 117: 624–631.

[45] Di Valentin C., Finazzi E., Pacchioni G., Selloni A., Livraghi S., Paganini MC, Giamello E., N-doped $TiO_2$: theory and experiment. *Chem. Phys*. 2007; 339 (1–3): 44–56.

[46] Mihailescu IN, Ristoscu C., Bigi A., Mayer I., Advanced biomimetic implants based on nanostructured coatings synthesized by pulsed laser technologies, Chapter 10. In: *Laser-Surface Interactions for New Materials Production Tailoring Structure and Properties*, Series: Springer Series in Materials Science, Vol. 130, Miotello A.; Ossi P.M. (Eds.), 2010, pp. 235–260.

[47] Schneider CW, Lippert T., Laser ablation and thin film deposition, Chapter 5. In: *Laser Processing of Materials Fundamentals, Applications and Developments*, Schaaf P. (Ed.), Springer Series in Materials Science 139, Berlin, 2010, pp. 89–112.

[48] Bauerle D., *Laser Processing and Chemistry*, Springer-Verlag, Berlin Heidelberg, 3rd ed., 2000.

[49] Mihailescu IN, Gyorgy E., Pulsed laser deposition: an overview. In: *International Trends in Optics and Photonics*, Asakura T. (Ed.), Heidelberg, Springer, 1999, pp. 201–2014.

[50] Eason R. (Ed.), *Pulsed Laser Deposition of Thin Films: Applications-led Growth of Functional Materials*, Wiley & Sons, 2007.

[51] Craciun D., Bourne G., Zhang J., Siebein K., Socol G., Dorcioman G., Craciun V. Thin and hard ZrC/TiN multilayers grown by pulsed laser deposition. *Surf. Coat. Technol.*, 2011; 205 (23–24): 5493–549.

[52] Ristoscu C., Mihailescu IN, Biomimetic coatings by pulsed laser deposition, Chapter 7. In: *Laser Technology in Biomimetics*, Schmidt V., Belegratis M.R. (Eds.), 2013, Basics and Applications, Series: Biological and Medical Physics, Biomedical Engineering, Springer-Verlag, Heidelberg, New York, Dordrecht, London, pp. 163–191.

[53] Socol G., Gnatyuk Y., Stefan N., Smirnova N., Sutan C., Malinovski V., Stanculescu A., Korduban O., Mihailescu I.N., Photocatalytic activity of pulsed laser deposited $TiO_2$ thin films in $N_2$, $O_2$ and $CH_4$. *Thin Solid Films* 2010; 518: 4648–4653.

[54] Oh S., Moon K.-S., Moon J.-H., Bae Ji-M., Jin S., Visible light irradiation-mediated drug elution activity of nitrogen-doped Ti $O_2$ nanotubes. *J. Nanomater.* 2013; 2013: Article ID 802318.

[55] Wang H., Hu Y., The photocatalytic property of nitrogen-doped $TiO_2$ nanoball film. *Int. J. Photoenergy* 2013; 2013: Article ID 179427.

[56] Linnik O., Shestopal N., Smirnova N., Eremenko A., Korduban O., Kandyba V., Kryshchuk T., Socol G., Stefan N., Popescu-Pelin G., Ristoscu C., Mihailescu IN, Correlation between electronic structure and photocatalytic properties of non-metal doped $TiO_2$/$ZrO_2$ thin films obtained by pulsed laser deposition method. *Vacuum.* 2015; 115: 166–171.

[57] Nakano Y., Morikawa T., Ohwaki T., Taga Y., Origin of visible-light sensitivity in N-doped $TiO_2$ films. *Chem. Phys.* 2007; 339: 20–26.

[58] Gnatuk Y., Smirnova N., Korduban O., Eremenko A., Effect of zirconium incorporation on the stabilization of $TiO_2$ mesoporous structure. *Surf. Interface Anal.* 2010; 42: 1276–1280.

[59] Chen H., Nambu A., Wen W., Graciani J., Zhong Z., Hanson JC, Fujita E., Rodriguez JA, Reaction of NH3 with titania: N-doping of the oxide and TiN formation. *J. Phys. Chem. C* 2007; 111 (3): 1366–1372.

[60] Linnik O., Petrik I., Smirnova N., Kandyba V., Korduban O., Eremenko A., Socol G., Stefan N., Ristoscu C., Mihailescu I. N., Sutan C., Malinovski V., Djokic V., Janakovic D., $TiO_2/ZrO_2$ thin films synthesized by PLD in low pressure N-, C- and/or O-containing gases: structural, optical and photocatalytic properties. *Digest J. Nanomater. Biostruct.* 2012; 7(3): 1343–1352.

[61] Katoh R., Furube A., Yamanaka K.-i, Morikawa T., Charge separation and trapping in N-doped $TiO_2$ photocatalysts: a time-resolved microwave conductivity study. *J. Phys. Chem. Lett.* 2010; 1 (22): 3261–3265.

[62] Dunnill CWH, Aiken ZA, Pratten J., Wilson M., Morgan DJ, Parkin IP, Enhanced photocatalytic activity under visible light in N-doped $TiO_2$ thin films produced by APCVD preparations using t-butylamine as a nitrogen source and their potential for antibacterial films. *J. Photochem. Photobiol. A: Chem.* 2009; 207 (2–3): 244–253.

[63] Oropeza FE, Harmer J., Egdell RG, Palgrave RG, A critical evaluation of the mode of incorporation of nitrogen in doped anatase photocatalysts. *Phys. Chem. Chem. Phys.* 2010; 12: 960–969.

[64] Braun A., Akurati KK, Fortunato G., Reifler FA, Ritter A., Harvey AS, Vital A., Graule T., Nitrogen doping of $TiO_2$ photocatalyst forms a second eg state in the oxygen 1s NEXAFS pre-edge. *J. Phys. Chem. C* 2010; 114 (1): 516–519.

IntechOpen